JOURNAL OF MOLECULAR SPECTROSCOPY 165, 303–314 (1994)

Double-Resonance Spectroscopy on Triplet States of CO

RIENK T. JONGMA,[1] MAARTEN G. H. BOOGAARTS, AND GERARD MEIJER

Department of Molecular and Laser Physics, University of Nijmegen, Toernooiveld, 6525 ED, Nijmegen, The Netherlands

Double-resonance spectroscopy is used to investigate the $v' = 2$ level of the $b^3\Sigma^+$ state and perturbing high vibrational levels ($v' = 40$–42) of the $a'^3\Sigma^+$ state of CO. Single rotational levels in the $a^3\Pi(v = 0)$ state are prepared via laser excitation on the Cameron band around 206 nm. Cavity-ring-down absorption spectroscopy is used to determine the absolute transition strength of this spin-forbidden transition; a value of $A_{0,0} = 41 \pm 10$ sec^{-1} is obtained. A laser-induced fluorescence study is performed on the metastable triplet state molecules in the region of the $2 \leftarrow 0$ band of the Third Positive System of CO. From the analysis of the interacting $^3\Sigma^+$ states deperturbed rotational and vibrational constants as well as interaction parameters of these states are obtained. Franck–Condon factors for the transition from $b^3\Sigma^+(v' = 2)$ and $(v' = 0)$ to the $a^3\Pi$ state are obtained from dispersion measurements.

1. INTRODUCTION

The Third Positive System (given by all transitions between the $b^3\Sigma^+$ state and the $a'^3\Sigma^+$ state in the 250–300 nm region) is one of the most intense spectral features of CO both in emission and in absorption (*1*). A detailed rotational analysis of many of the vibrational bands of this system appeared in the early days of molecular spectroscopy. The rotational structures of both the $b^3\Sigma^+(v' = 0)$ (*2*) and the $(v' = 1)$ state (*3*) were determined in that period. A strong interaction with high vibrational levels of the $a'^3\Sigma^+$ state complicated the analysis of these states (*4*).

In 1930, Kaplan reported on "A New System of Bands in Carbon Monoxide" (*5*) which he attributed to the intercombination band of a metastable quintet state with the $a^3\Pi$ state. A few years later, Schmid and Gerö (*6*) speculated that the upper state of this transition is actually the perturbed $v' = 2$ level of the $b^3\Sigma^+$ state. It was only in 1987 that this latter assignment was concluded to be correct on the basis of a detailed analysis of the isotope effect on the frequency positions of the bands as well as on the basis of observed vibrational band intensities in medium-resolution emission spectra of a hollow cathode CO discharge (*7*). Rotational analysis of the $b^3\Sigma^+(v' = 2)$ state and an analysis of the perturbations were reported in 1992 by Rytel (*8*), who photographed the 2–2 band of the Third Positive System at high resolution.

In this paper we report rotational-state-resolved measurements of the $b^3\Sigma^+(v' = 2)$ state and the perturbing $a'^3\Sigma^+(v' = 40$–$42)$ states using double-resonance laser excitation and fluorescence detection. Single rotational levels in the $v = 0$ level of the lower state of the Third Positive System are prepared via laser excitation on the $a^3\Pi(v = 0) \leftarrow X^1\Sigma^+(v'' = 0)$ transition; cavity-ring-down absorption spectroscopy is used to determine the absolute transition strength of this spin-forbidden transition.

[1] E-mail: rienkj@sci.kun.nl.

0022-2852/94 $6.00

The metastable triplet state molecules are further excited to the $b^3\Sigma^+(v' = 2)$ level and the perturbing levels of the $a'^3\Sigma^+$ state using tunable 250 nm radiation. A schematic representation of the excitation process is given in Fig. 1. Absolute energies of the $^3\Sigma^+$ states are determined and modelled using a nearly Hund's case (b) description, including the strong $^3\Sigma^+$–$^3\Sigma^+$ interaction. From the analysis of the interacting $^3\Sigma^+$ states, deperturbed rotational and vibrational constants as well as interaction parameters are obtained. Dispersed fluorescence from the upper states is measured to determine the Franck–Condon factors for the transition from the $b^3\Sigma^+(v' = 2)$ and $(v' = 0)$ levels to the $a^3\Pi$ state.

2. EXPERIMENTAL SETUP

To induce the $a^3\Pi(v = 0) \leftarrow X^1\Sigma^+(v'' = 0)$ transition around 206 nm, a pulsed dye laser system (Spectra Physics, PDL-3) operating on Sulforhodamine 640, pumped by a frequency doubled Nd:YAG laser (GCR-11), is used. The radiation of the dye laser (618 nm, 35 mJ/pulse, 0.05 cm^{-1} bandwidth) is frequency-doubled in a KDP-crystal. The fundamental and the second harmonic radiation are mixed in a BBO-crystal, thus producing pulsed tunable radiation around 206 nm with a power of several tenths of a mJ and a bandwidth of approximately 0.5 cm^{-1}. The relatively poor bandwidth of the tripled laser radiation is most likely caused by the irregular temporal profile of the (noninjection seeded) Nd:YAG pump laser.

To determine the strength of the $a^3\Pi(v = 0) \leftarrow X^1\Sigma^+(v'' = 0)$ transition, sensitive direct absorption measurements are performed using cavity-ring-down spectroscopy. Cavity-ring-down spectroscopy was introduced as a sensitive direct absorption technique to be used with pulsed lasers (*9*) and was recently shown to be applicable to the UV region of the spectrum as well (*10*). The method is based upon the measurement of the rate of absorption rather than the magnitude of absorption of a light pulse confined within a closed optical cavity. This means that rather than measuring the

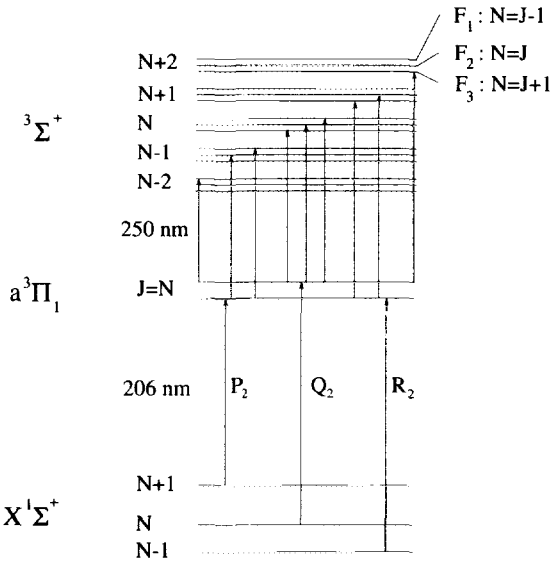

FIG. 1. Double-resonance $^3\Sigma^+ \leftarrow a^3\Pi_1 \leftarrow X^1\Sigma^+$ excitation scheme. Allowed rotational transitions after P_2, Q_2, and R_2 excitation in the Cameron band are indicated.

decrease in transmitted intensity due to absorption of the sample, the decrease in the Q-factor of the cavity due to the absorption is measured by recording the temporal profile of the transmitted radiation with a fast digitizer. By measuring the so-called cavity-ring-down time instead of the absolute transmitted intensity, problems due to pulse-to-pulse fluctuations in the radiation source, which are often the limiting factor in direct absorption experiments, are circumvented.

The cavity-ring-down experiments are performed in a stable optical cavity of 44-cm length using two plano-concave, 1-in.-diameter mirrors with a radius of curvature of 25 cm. The cavity can be evacuated by a rotary-pump/cryo-pump combination; experiments are performed with a few Torr of CO in the cell. The mirrors are coated for maximum reflectivity at 206 nm (Laseroptik GmbH, Garbsen, Germany). The actual reflectivity at this wavelength is accurately determined from the observed cavity ring down time of the empty cavity as $R = 98.45\%$, corresponding to a 95-nsec decay time.

A small fraction of the frequency-tripled laser light (several nJ/pulse) is coupled into the optical cavity via one of the mirrors. The time-dependent transmitted radiation intensity is detected by a photomultiplier and digitized by and displayed on an oscilloscope with a 100-MHz sampling rate and a 10-bit vertical resolution (LeCroy 9430). The signal is added over a number of laser shots (typically 25) into a 16-bit memory at a fixed wavelength setting of the laser and the summed signal is recorded by a PC. After the background is subtracted the natural logarithm of the data is taken and fit (using a least-squares-weighted fitting algorithm (*11*)) to a straight line. Using this setup, the cavity decay time at a given wavelength can be determined with a standard deviation of 0.3 nsec, i.e., a relative accuracy of 0.3%. With the measured reflectivity of 98.45%, this translates into a minimum detectable absorption of 5×10^{-5} per pass through the cavity. So even in the UV region of the spectrum, where no better mirrors than the ones we used are yet available, absorption signals that are less than 10^{-3} of the pulse-to-pulse intensity fluctuation of the radiation source that is used can be detected by this technique.

The double-resonance measurements are performed in a standard laser-induced fluorescence (LIF) cell. In the measurements stationary CO at room temperature and at a pressure of 1 Torr or less is used. The 206-nm laser light is now produced via frequency tripling of the radiation of a PDL-2 dye laser system in an otherwise identical scheme, yielding 0.15 mJ/pulse with a bandwidth of approximately 1 cm^{-1}. The 250-nm radiation needed to induce the $^3\Sigma^+ \leftarrow a^3\Pi(v = 0)$ transitions is produced via anti-Stokes Raman shifting of the frequency doubled output of the PDL-3 laser, operating on Fluorescein 548. The PDL-3 system is used to generate the 250-nm radiation as it has better spectral resolution. The anti-Stokes Raman shifting is performed by focusing the frequency-doubled dye laser with a 20 cm focal length lens in a 25 cm long H_2 cell at 13 bar. The Raman shift under these experimental conditions is equal to 4155.22 cm^{-1} (*12*). The absolute frequency of the 250-nm radiation is calibrated via simultaneous recording of the I_2 absorption spectrum at the fundamental wavelength of the dye laser (*13*). Less than 5 μJ of the 250-nm radiation (0.4-cm^{-1} bandwidth) is coupled into the LIF cell through calibrated absorption filters to prevent saturation effects. The lasers are counter-propagating through the LIF cell. Laser-induced fluorescence on the $^3\Sigma^+(v', N') \rightarrow a^3\Pi(v'', J'')$ transition is detected by a photomultiplier and recorded by the oscilloscope–computer system. This system is used as an advanced boxcar-integrator system (detection gates can be set by the software) and is used to control the laser wavelength as well. To reduce the stray light of

both lasers, a 2-mm UG-5 filter (Schott) is placed in front of the photomultiplier. To reduce remaining background signal, fluorescence detection started some tens of nsec after the second laser had fired. Time delay between the two lasers, and triggering of the entire system is controlled by a delay generator (DG535, Stanford Research Systems Inc.). A monochromator-based fluorescence detection system is used for recording the fluorescence spectrum in dispersion.

3. RESULTS AND DISCUSSION

The upper curve in Fig. 2 shows the absorption spectrum of 1.5 Torr CO as measured via cavity-ring-down spectroscopy. The vertical scale is in percent intensity loss per pass; the baseline is at 1.55%, indicating a mirror reflectivity of 98.45%. Shown in this figure is the Q_3 branch of the $a^3\Pi(v = 0) \leftarrow X^1\Sigma^+(v'' = 0)$ of the Cameron band. The intensity distribution in the Cameron band is governed by the mixing of the $A^1\Pi$ state with the $a^3\Pi$ state, making only transitions from the electronic ground state to the $a^3\Pi_1$ spin–orbit component of the triplet state possible, in a pure Hund's case (a) description (*14*). As the $a^3\Pi$ state of CO is best described as an intermediate case (between (a) and (b)) there is a considerable degree of mixing of the various multiplet components (*15*). This mixing increases for increasing J values, making transitions to, for instance, the $a^3\Pi_2$ multiplet component (F_3 level) possible as well, as explicitly demonstrated in the figure. From a comparison of the measurements to the calculated cavity-ring-down spectrum, shown as the lower trace in Fig. 2, it is concluded that the

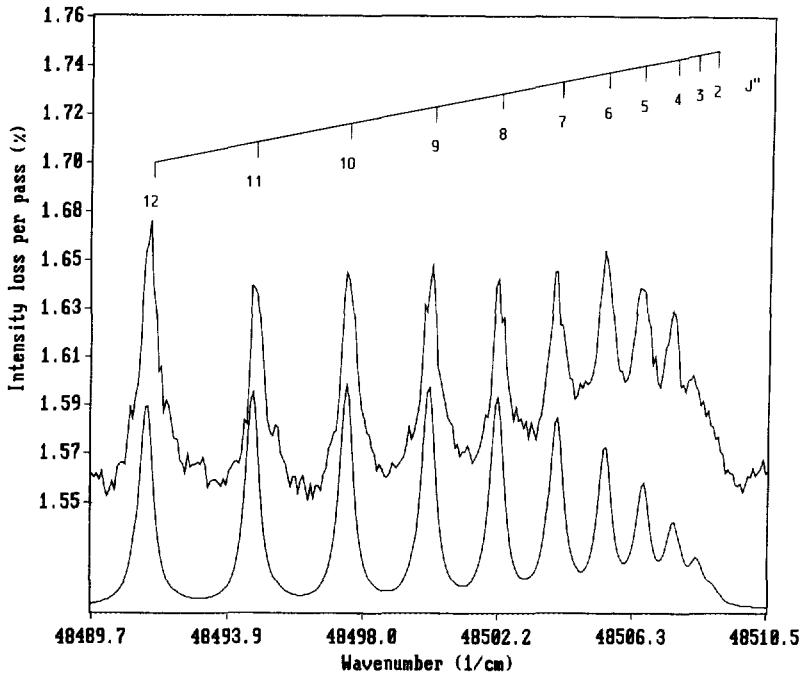

FIG. 2. Room-temperature absorption spectrum of the Q_3 branch of the $0 \leftarrow 0$ Cameron band of CO at 1.5 Torr in a 44-cm-length cavity as measured via cavity-ring-down spectroscopy around 206 nm (upper trace) together with a simulated spectrum with $A_{0,0} = 41\ \text{sec}^{-1}$ (lower trace). The vertical scale is in percent intensity loss per pass.

intensity distribution is indeed governed by the suggested mechanism for values of J up to $J = 15$. An Einstein A coefficient for the $0 \leftarrow 0$ transition of $A_{0,0} = 41 \pm 10$ sec^{-1} is deduced from the observed line intensities in combination with the known rotational ground state distribution at room temperature (*16*), the known pressure in the cell, and the absorption pathlength. The A coefficient is determined assuming a Lorentzian laser profile with a bandwidth of 0.5 cm^{-1} (FWHM) and a Doppler width (FWHM) of the CO lines of 0.11 cm^{-1} (*17*). For higher values of J, a clear deviation from the expected intensity distribution is observed, and a more detailed analysis of the observed intensity distribution is underway. This value of the Einstein A coefficient implies that in the double resonance experiments, where we used approximately 0.15 mJ of 206-nm light in a 2.5-mm-diameter beam, the excitation efficiency for the strongest rotational lines in the Cameron band is about 10^{-5}.

The energy levels that can be reached in the upper $^3\Sigma^+$ states by the double-resonance excitation are restricted to relatively low values of N for various reasons. First, there is the restriction due to the room-temperature Boltzmann distribution of the CO population in the ground state, causing the $N = 7$ level to have the maximum population of 8.3%. Second, the intensity distribution in the weak Cameron band is mainly concentrated in transitions to the $a^3\Pi_1$ multiplet component for low rotational quantum numbers, while it is distributed over more transitions at higher quantum numbers. This intensity distribution favors efficient preparation of levels with low quantum numbers in the $a^3\Pi_1$ component. Last, but not least, the transitions from the $a^3\Pi$ state to high vibrational levels of the $a'\ ^3\Sigma^+$ are very weak due to small Franck–Condon factors, and only gain intensity due to the interaction with the $b^3\Sigma^+$ state, which is sufficient to make them observable for only a selected set of levels.

In Fig. 3 a typical laser excitation spectrum of rotational transitions in the $a'\ ^3\Sigma^+(v' = 42) \leftarrow a^3\Pi(v = 0)$ band is shown. The 0.4-cm^{-1} bandwidth of the laser determines the observed linewidth in this spectrum. The absolute frequency position of unblended lines can be determined with a 0.06-cm^{-1} accuracy. Rotational selection rules dictate that only rotational levels in the upper $^3\Sigma^+$ state with $\Delta N = 0, \pm 2$ relative to the

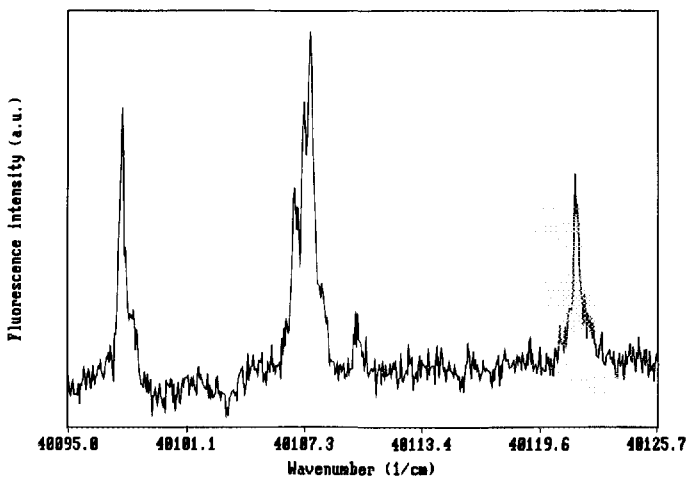

FIG. 3. Double-resonance excitation spectrum to the $a'\ ^3\Sigma^+(v' = 42)$ state starting from the laser prepared $a^3\Pi_1(v = 0, J = 5)$ plus-parity level. Transitions to $N' = 3$, 5, and 7 are seen in this spectrum. The spin splitting of the $N' = 5$ level is barely resolved.

starting rotational level in the electronic ground state can be reached, as explicitly indicated in Fig. 1. As in most of the measurements, preparation of a single Λ-doublet component in the $a^3\Pi_1$ state is achieved by excitation on a Q_2 transition; in the measurement presented in Fig. 3 this is the $Q_2(5)$ transition. As can be inferred from Fig. 1, the various transitions appearing in this spectrum in order of increasing frequency are the ${}^{O}P_{12}(5)$, the barely resolved triplet ${}^{Q}Q_{22}(5)$, ${}^{Q}R_{12}(5)$, ${}^{Q}P_{32}(5)$, and the ${}^{S}R_{32}(5)$, where the notation ${}^{\Delta N}\Delta J_{F_{\text{upper}}F_{\text{lower}}}(J_{\text{lower}})$ is used. The weak additional peak around 40 110 cm^{-1} is due to simultaneous population of the $a^3\Pi_1(v = 0, J = 6)$ level via the $Q_2(6)$ transition in the wing of the laser profile. Excitation on the Q_2 lines has the advantage that fully isolated F_1 and F_3 levels in the ${}^3\Sigma^+$-states are reached. In some cases P_2 lines have been used for the first excitation step, resulting in two doublets in the double-resonance spectrum, as is evident from Fig. 1.

Double-resonance experiments involving transitions to various rotational levels in the $b^3\Sigma^+(v' = 2)$ level and in the $a'\,{}^3\Sigma^+(v' = 40\text{–}42)$ levels have been performed. Rotational transitions have been selected so as to yield the most accurate and complete information on the energy level structure of the upper ${}^3\Sigma^+$ states. The measured transitions from the $a^3\Pi(v = 0)$ to the $a'\,{}^3\Sigma^+$ and $b^3\Sigma^+$ state are tabulated in Tables I and II.

In addition to these laser excitation spectra in which the total fluorescence from the upper ${}^3\Sigma^+$ state is collected, dispersed-fluorescence measurements have been performed to obtain insight in the vibrational intensity distribution of the CO fluorescence. A typical dispersion spectrum together with the assignment of the various vibrational transitions is given in Fig. 4. This dispersion spectrum is obtained after double-resonance excitation on the $Q_2(6)$ and the ${}^{S}R_{32}(6)$ lines, thus populating the isolated F_3 spin component of the $N' = 8$ rotational level in the $b^3\Sigma^+(v' = 2)$ state. This level is at an absolute energy of 88 248.66 cm^{-1} relative to the $(v'' = 0, N'' = 0)$ level in the electronic ground state of CO. In addition to the direct emission from the $v' = 2$ level, emission from lower vibrational levels in the $b^3\Sigma^+$ state, levels that are populated via collisional energy transfer, is observed as well. It is clear from this emission spectrum that collisional energy redistribution takes place within the radiative lifetime of the excited state ($\tau_{v'=2} \geqslant 20$ nsec) under the experimental conditions we employed. It is not clear, therefore, if the fluorescence we detect from the $a'\,{}^3\Sigma^+$ state only results from the partial $b^3\Sigma^+$ character of the $a'\,{}^3\Sigma^+$ state or if it also in part results from collisional redistribution to the $b^3\Sigma^+$ state.

4. ANALYSIS

One of the aims of this study is to accurately determine the rotational structure of the mutually perturbing ${}^3\Sigma^+$ states. Therefore, the observed rotational transitions as

TABLE I

Observed Lines of the ${}^3\Sigma^+ \leftarrow a^3\Pi(v = 0)$ Transition Using P_2 Lines to Prepare the Single Rotational Levels in the Metastable ${}^3\Pi$ State

State	J	${}^{P}Q_{12}(J)$	${}^{P}P_{22}(J)$	${}^{R}R_{22}(J)$	${}^{R}Q_{32}(J)$
$a'^3\Sigma^+(v=41)$	4	39851.04±0.15	39851.04±0.15	39863.66±0.15	39863.66±0.15
	5	839.95±0.15	839.95±0.15	855.67±0.15	855.67±0.15
	6	826.88±0.15	826.88±0.15	845.93±0.15	845.93±0.15
	7	812.07±0.15	812.07±0.15	834.38±0.06	834.96±0.06
	8	795.73±0.08	795.31±0.08	822.48±0.06	823.12±0.06
	9	778.00±0.08	777.66±0.08	810.33±0.06	810.91±0.06
$b^3\Sigma^+(v=2)$	4	39654.00±0.15	39654.00±0.15	39679.98±0.15	39679.98±0.15
	6			680.90±0.15	680.90±0.15

TABLE II

Observed Lines of the $^3\Sigma^+ \leftarrow a^3\Pi(v = 0)$ Transition Using Q_2 Lines to Prepare the Single Rotational Levels in the Metastable $^3\Pi$ State

State	J	$^{O}P_{12}(J)$	$^{Q}R_{12}(J)$	$^{Q}Q_{22}(J)$	$^{Q}P_{32}(J)$	$^{S}R_{32}(J)$
$a'^3\Sigma^+(v=40)$	2	39491.31±0.06	39496.31±0.10	39496.55±0.10	39496.70±0.10	39507.70±0.06
	3	482.98±0.06	491.27±0.10	490.71±0.10	491.43±0.10	505.41±0.06
	4	473.10±0.06	484.17±0.10	483.79±0.10	484.43±0.10	501.12±0.06
	5	461.24±0.06	475.33±0.10	474.75±0.06	475.47±0.10	495.54±0.06
	6		464.18±0.10	463.74±0.06	464.46±0.10	485.99±0.06
	11	347.59±0.08	375.26±0.10	374.82±0.10	375.58±0.10	407.24±0.08
$a'^3\Sigma^+(v=41)$	2	39866.08±0.06	39870.23±0.10	39870.55±0.10	39870.68±0.10	39879.98±0.06
	3	857.49±0.06		863.72±0.10	64.56±0.10	876.84±0.06
	4	846.96±0.06	856.37±0.10	856.01±0.10	856.69±0.10	872.06±0.06
	5	834.32±0.06	846.68±0.10	846.26±0.10	846.92±0.10	865.76±0.06
	6	819.81±0.06	835.17±0.10	834.77±0.06	835.39±0.10	858.05±0.06
	7	803.31±0.06	822.11±0.10	821.73±0.06	822.37±0.06	849.52±0.06
	8	785.06±0.06		807.42±0.06	807.98±0.10	840.70±0.06
	9	765.34±0.06		792.12±0.06	792.72±0.06	
	16			707.09±0.10		
$a'^3\Sigma^+(v=42)$	2	40132.32±0.06	40135.65±0.10		40136.23±0.10	40143.47±0.06
	3	132.57±0.06			129.27±0.10	138.75±0.06
	5	098.93±0.06	108.43±0.06	40107.97±0.06	108.82±0.06	122.67±0.06
	6	083.15±0.06	094.85±0.10	094.46±0.06	095.20±0.06	111.16±0.06
	11	39969.99±0.06	39993.03±0.10	39992.61±0.06	39993.42±0.10	021.90±0.06
	13	909.26±0.06				39974.29±0.06
$b^3\Sigma^+(v=2)$	1					39683.94±0.06
	2	39660.00±0.06	39668.70±0.10		39668.75±0.10	688.81±0.06
	3	652.94±0.06	667.27±0.06			693.32±0.06
	4					697.39±0.06
	13	548.02±0.06		39600.61±0.15		649.19±0.06

given in Tables I and II are reduced to the absolute energies of the rotational levels in these states. For this, the observed transition frequencies are combined with the known rotational structure in the $X^1\Sigma^+(v'' = 0)$ electronic ground state (*16*) and with the tabulated (calculated) absolute transition frequencies of the Cameron band (*15*). The error in the thus determined absolute energies is on the order of 0.1 cm^{-1}. The transitions of the 2 ← 2 band of the Third Positive System as reported by Rytel (*8*) are reduced in the same way to yield additional values for the energy levels that are also included in the fit.

Modeling of the rotational structure and the mutual interaction of the excited $^3\Sigma^+$ states is most accurately performed starting from the Hund's case (b) formalism. It should be explicitly noted that this is possible in our case as the energy levels of the $^3\Sigma^+$ states are fitted rather than the $^3\Sigma^+ \leftarrow a^3\Pi$ transition frequencies.

In the model we use (*18*), the spin-splitting is treated as a small perturbation of the case (b) rotational energy levels of the $^3\Sigma^+$ states. The total energy $F_J(N)$ of a rotational level in the $^3\Sigma^+$ states is given by

$$F_J(N) = T_J(N) + \mathscr{H}^{c}_J(J) + \mathscr{H}^{sr}_J(J). \quad (1)$$

In this expression N is the quantum number for the end-over-end rotation of the CO molecule, whereas J is the total angular momentum quantum number, containing information on the coupling of **N** with the electron spin **S** via $\mathbf{J} = \mathbf{N} + \mathbf{S}$. When used as a subscript, J is a label to identify the spin multiplet components belonging to a given N; the labels are $J - 1$, J, and $J + 1$ for F_1 ($N = J - 1$), F_2 ($N = J$), and F_3 ($N = J + 1$) components, respectively. In $T_J(N)$ the term value $\nu_0(v)$ (i.e., the absolute energy of the (v, $N = 0$) level in the $^3\Sigma^+$ state relative to the ($v'' = 0$, $N'' = 0$) level in

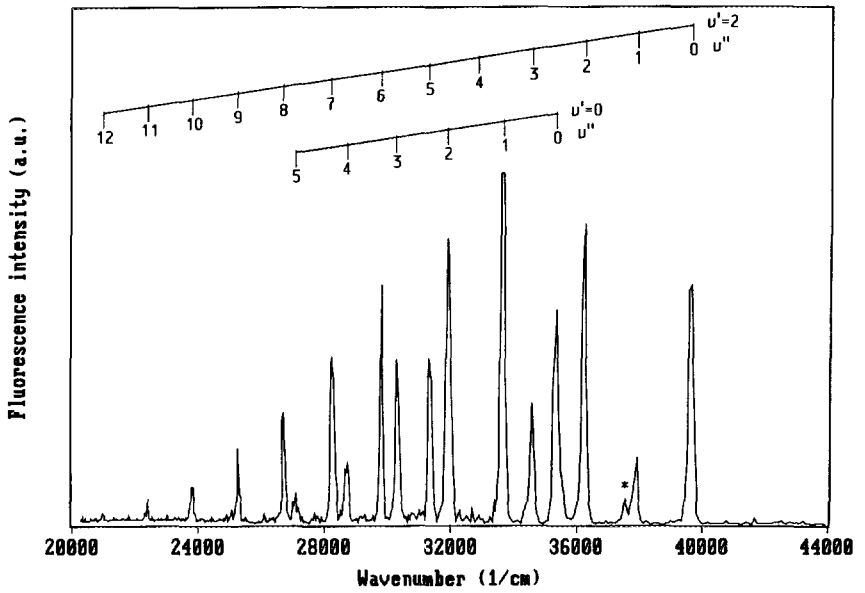

FIG. 4. Dispersed laser-induced $b^3\Sigma^+(v') \rightarrow a^3\Pi(v'')$ fluorescence spectrum of CO. The $b^3\Sigma^+(v' = 2, N' = 8)$ F_3 level is excited and vibrational assignment of the resulting fluorescence is made in the figure. The peak indicated with an asterisk is due to the $v' = 1 \rightarrow v'' = 0$ transition in the Third Positive System.

the electronic ground state of CO) the rotational energy (rotational constant $B(v)$) and the spin–spin interaction (coupling parameter $\epsilon(v)$) are included via

$$T_{J-1}(N) = \nu_0(v) + B(v)\Big[N(N+1) + (2N+3) - \sqrt{\frac{3\epsilon(v)}{B(v)}\left(\frac{3\epsilon(v)}{4B(v)} - 1\right) + (2N+3)^2}\Big] - \frac{\epsilon(v)}{2}$$

$$T_J(N) = \nu_0(v) + B(v)N(N+1) + \epsilon(v)$$

$$T_{J+1}(N) = \nu_0(v) + B(v)\Big[N(N+1) - (2N-1) + \sqrt{\frac{3\epsilon(v)}{B(v)}\left(\frac{3\epsilon(v)}{4B(v)} - 1\right) + (2N-1)^2}\Big] - \frac{\epsilon(v)}{2}. \quad (2)$$

The last two terms in the Eq. (1) describe the contribution of the centrifugal distortion (distortion parameter $D(v)$) and the contribution of the spin–rotation interaction $\mathbf{N}\cdot\mathbf{S}$ (interaction parameter $\gamma(v)$) to the total energy and have the explicit forms

$$\mathscr{H}^{c}_{J\mp1}(J) = -\frac{D(v)}{u^{\pm}(J)^2 + 4J(J+1)}(4J^2(J+1)^2[J(J+1)+4 - 16J(J+1)+1]u^{\pm}(J) + [(J(J+1)+4)2 - 12]u^{\pm}(J)^2)$$

$$\mathscr{H}^{sr}_{J\mp1}(J) = -\gamma\left(1 + u^{\pm}(J)\frac{u^{\pm}(J) - 4J(J+1)}{u^{\pm}(J)^2 + 4J(J+1)}\right), \quad (3)$$

with

$$u^{\pm}(J) = \frac{3\epsilon(v)}{2B(v)} - 1 \pm \sqrt{\frac{3\epsilon(v)}{B(v)}\left(\frac{3\epsilon(v)}{4B(v)} - 1\right) + (2J+1)^2}. \qquad (4)$$

To calculate the true values of the energy levels in the $^3\Sigma^+$ states the interaction between the b and the a' state has to be taken into account. Interaction can only occur between levels that have the same total angular momentum quantum number J and the same symmetry (*18*). For the $^3\Sigma^+$ states the symmetry of the levels is determined by the parity, which is given by $(-1)^{N+J}$. The levels can therefore be subdivided in two groups, named e and f levels, of which the former have a positive symmetry (F_2 levels) whereas the latter change sign upon reflection in the origin (F_1 and F_3 levels). In principle a $\Delta N = 2$ interaction between the F_1 and F_3 f levels is present. Such an interaction was included in our fit but did not improve the quality of the fit and the corresponding interaction parameter was too small to be determined. This is not too surprising as a $\Delta N = 2$ interaction is strictly forbidden in pure Hund's case (b).

As the $\Delta N = 2$ interaction is neglected in the further analysis, a separate energy matrix can be set up for each spin-multiplet component F_i belonging to a certain N. The diagonal elements of this matrix contain the energy of the $b^3\Sigma^+(v = 2)$ state and the various interacting vibrational levels of the $a'\,^3\Sigma^+$ state. The off-diagonal elements take the interaction between the $b^3\Sigma^+(v = 2)$ and the $a'\,^3\Sigma^+(v)$ state into account and are denoted by $\zeta(2, v)$. This interaction between the $^3\Sigma^+$ states is independent of the rotational quantum numbers.

The model presented here is used in a fit procedure to determine the relevant spectroscopic constants. The fit procedure uses the energy values of the $b^3\Sigma^+(v' = 2)$ and of the $a'\,^3\Sigma^+(v' = 40\text{–}42)$ states. The influence of the $a'\,^3\Sigma^+(v' = 39)$ and $(v' = 43)$ are included in the fit by extrapolation of the fitted constants for $v' = 40\text{–}42$ to get more reliable results, although no direct measurements of energy levels belonging to either of these states have been performed. The spin-splitting parameters of these nonmeasured vibrational states are not included as they will hardly influence the energy value of the other states.

Using all the transitions given in Tables I and II, the measurements can be reduced to yield 72 new energy levels in the $^3\Sigma^+$ states. Including the transitions as reported by Rytel (*8*), a total of 134 energy levels are fitted in a least-squares fitting algorithm to a set of 20 variables. It should be noted that the energy levels calculated from the data by Rytel had to be lowered by 0.12 cm^{-1} to be in agreement with our own measurements of the same levels. This slight discrepancy might be caused by a systematic shift of the calculated energy levels in $a^3\Pi(v = 2)$ relative to $a^3\Pi(v = 0)$ (*15*).

The fitted constants are given in Table III. The error indicated for the various constants is one time the standard deviation. The standard deviation of the total fit is 0.017 cm^{-1}, and the maximum deviation between calculated and observed energy levels is 0.1 cm^{-1}, still within the experimental error for that specific level. The energy level calculated from the $^QQ_{33}(13)$ transition as given by Rytel at 36 175.32 cm^{-1} is excluded from the fit as this locates the $b^3\Sigma^+(v' = 2, N' = 14)$ F_3 level 0.25 cm^{-1} below our calculated value. Comparison of our fitted constants to the constants determined by Rytel (*8*) is complicated by the fact that different models have been used to describe the energy level structure in the perturbing states.

In Fig. 5 the measured energy levels in the $^3\Sigma^+$ states are plotted as a function of $N(N + 1)$. The spin-splitting of the different N levels is too small to be observable in

TABLE III

Spectroscopic Constants of the $a'\,^3\Sigma^+(v' = 39\text{–}43)$ and the $b^3\Sigma^+(v' = 2)$ States as Obtained from the Fit

State	$\nu_0(v)$ [b]	B(v)	D(v)·10^5	$\epsilon(v)\cdot10^2$	$\gamma(v)\cdot10^4$	$\zeta(2,v)$
$a'^3\Sigma^+$(v=39)	87662.8[a]	0.59373[a]				80.97[a]
(v=40)	88014.277±0.16	0.56923±0.0013		-44.70±1.7	-79.7±10	74.951±0.118
(v=41)	88329.634±0.017	0.53864±0.0004	1.515±0.18	-43.31±0.8	-130.2± 9	68.955±0.006
(v=42)	88609.181±0.03	0.50193±0.0004	2.194±0.17	-42.38±1.6	-181.8±10	62.926±0.080
(v=43)	88852.8[a]	0.45911[a]				56.89 [a]
$b^3\Sigma^+$(v=2)	88127.504±0.19	1.87194±0.0013	3.167±0.42		29.0± 6	

Note. The indicated error corresponds to one standard deviation in the fitted constants. A total of 134 energy levels are fitted with a standard deviation of the total fit of 0.017 cm^{-1}.

[a] Extrapolated values from $a'\,^3\Sigma^+(v' = 40\text{–}42)$.

[b] The error in ν_0 is determined by the fit and is equal to the relative error in $\nu_0(v)$. The error in the absolute value of ν_0 is 0.1 cm^{-1}.

this figure. The deperturbed energies as calculated from the fitted constants are indicated by dashed lines in the figure.

The Franck–Condon factors for transitions from the $b^3\Sigma^+(v' = 2)$ and $(v' = 0)$ to the $a^3\Pi$ state are determined from the dispersion spectrum shown in Fig. 4. This dispersion spectrum is measured after excitation of CO to the F_3 component of the $v' = 2$, $N' = 8$ level in the $b^3\Sigma^+$ state. The intensity of the fluorescence signal, $I_{em}^{v',v''}$, is proportional to

$$I_{em}^{v',v''} \sim \nu^4 N_{v'} |M_{el}(\bar{R})|^2 \left| \int \Psi_{v'} \Psi_{v''} dr \right|^2, \tag{5}$$

in which ν is the frequency of the given $v' \rightarrow v''$ transition, $N_{v'}$ is the population of the upper level, $M_{el}(\bar{R})$ is the electric dipole moment of the transition, and $|\int \Psi_{v'} \Psi_{v''} dr|^2$ is the corresponding Franck–Condon factor.

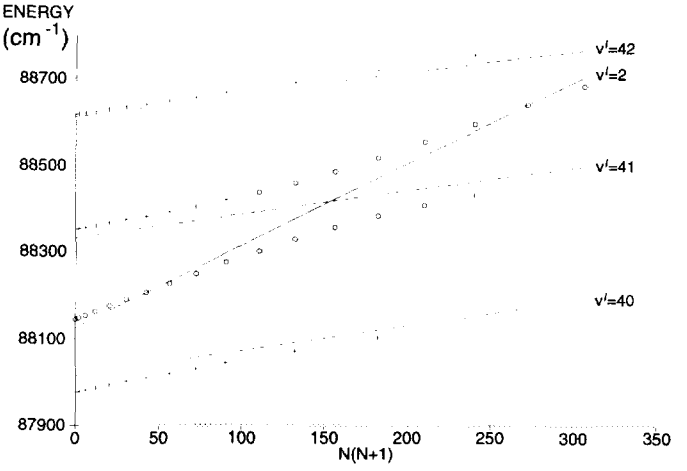

FIG. 5. Energy levels for the $^3\Sigma^+$ states as determined in this work (+) together with the levels as determined from other measurements (8) (O) as a function of $N(N + 1)$. The spin splitting is not indicated in this figure. The dashed lines indicate the calculated unperturbed rotational energies of the $a'\,^3\Sigma^+(v' = 40\text{–}42)$ and of the $b^3\Sigma^+(v' = 2)$ levels.

The spectral sensitivity of the detection system is mainly determined by the wavelength dependent detection efficiency of the photomultiplier that is used. To a good approximation, the quantum efficiency of the photomultiplier system is constant over the wavelength region in which the dispersion spectrum as shown in Fig. 4 is recorded. This means that the fluorescence intensity as measured by our detection system is approximately proportional to $I_{em}^{v',v''}/\nu$, i.e., proportional to $\nu^3 |\int \Psi_{v'} \Psi_{v''} dr|^2$.

In Fig. 4 vibrational progressions starting from the laser prepared $b^3\Sigma^+(v' = 2)$ level as well as from the collisionally populated $(v' = 0)$ level are seen. In addition, the $b^3\Sigma^+(v' = 1) \rightarrow a^3\Pi(v = 0)$ transition, indicated by an asterisk in the figure, is barely visible.

The Franck–Condon factors that are determined from these dispersion spectra are given in Table IV. They are normalized to unity for each vibrational progression. The values are compared to earlier calculated Franck–Condon factors (*7*) in the last column of the table. From this it is seen that the experimentally determined Franck–Condon factors for the $v' = 0$ progression agree very well with the calculated ones, whereas the observed $v' = 2$ intensity progression agrees only qualitatively (there are two nodes in the emission progression, reflecting the shape of the $v' = 2$ wavefunction) with the calculations. The discrepancy between experimentally determined and calculated Franck–Condon factors for the $v' = 2$ progression is most likely due to problems in correctly describing the wavefunction of the $v' = 2$ level using the limited set of available vibrational and rotational constants. In addition, the approximation of an R-independent transition dipole moment might not be correct. The presence of only one $v' = 1$ transition is in qualitative agreement with the calculated Franck–Condon factors.

The way in which the population from the $b^3\Sigma^+(v' = 2)$ level is redistributed in collisions is rather unexpected. It appears from dispersion spectra as shown in Fig. 4

TABLE IV

Measured and Calculated (*7*) Franck–Condon Factors of the $b^3\Sigma^+(v' = 2) \rightarrow a^3\Pi(v'')$ and $b^3\Sigma^+(v' = 0) \rightarrow a^3\Pi(v'')$ Transitions of the Third Positive System of CO

$b^3\Sigma^+(v') \rightarrow a^3\Pi(v'')$	This work	Calc.
2→ 0	0.05±0.02	0.32
2→ 1	0.03±0.01	0.11
2→ 2	0.14±0.02	0.17
2→ 3	0.07±0.01	0.02
2→ 4	0.01±0.01	0.02
2→ 5	0.08±0.01	0.08
2→ 6	0.17±0.02	0.12
2→ 7	0.14±0.02	0.10
2→ 8	0.11±0.02	0.07
2→ 9	0.08±0.02	
2→10	0.05±0.01	
2→11	0.04±0.02	
2→12	0.02±0.01	
0→ 0	0.16±0.06	0.20
0→ 1	0.28±0.01	0.29
0→ 2	0.28±0.03	0.24
0→ 3	0.16±0.02	0.15
0→ 4	0.08±0.02	0.08
0→ 5	0.05±0.02	0.04

Note. For each progression the Franck–Condon factors are normalized to unity.

that the collisional energy redistribution from $v' = 2$ to $v' = 0$ is preferred over the $v' = 2$ to $v' = 1$ redistribution. This suggests that resonance effects play an important role in this energy redistribution process; the $v' = 2 \rightarrow v' = 0$ transition in the $b^3\Sigma^+$ state is isoenergetic with the $v'' = 2 \leftarrow v'' = 0$ transition in the $X^1\Sigma^+$ ground state CO (the main collision partner), whereas the $v' = 2 \rightarrow v' = 1$ transition in the $b^3\Sigma^+$ state has a considerable energy mismatch with the $v'' = 1 \leftarrow v'' = 0$ transition in $X^1\Sigma^+$ CO.

5. CONCLUSIONS

Cavity-ring-down absorption spectroscopy has been employed to determine the absolute transition strength of the spin-forbidden $a^3\Pi(v = 0) \leftarrow X^1\Sigma^+(v'' = 0)$ Cameron band in CO. A value of $A_{0,0} = 41 \pm 10\ \text{sec}^{-1}$ is obtained, in good agreement with earlier measurements (*19*) and somewhat lower than the calculated value (*14*).

The $v' = 2$ level of the $b^3\Sigma^+$ state and perturbing high vibrational levels ($v' = 40$–42) of the $a'^3\Sigma^+$ state of CO are investigated using double-resonance laser excitation and fluorescence detection. Absolute energies of the $^3\Sigma^+$ states are determined and modelled using a nearly Hund's case (b) description, including the strong $^3\Sigma^+$–$^3\Sigma^+$ interaction. From the analysis of the interacting $^3\Sigma^+$ states deperturbed rotational and vibrational constants as well as interaction parameters are obtained. Franck–Condon factors for the $b^3\Sigma^+(v' = 2)$ and $(v' = 0)$ to the $a^3\Pi$ state are obtained from dispersion measurements.

RECEIVED: October 20, 1993

REFERENCES

1. P. H. KRUPENIE, "The Band Spectrum of Carbon Monoxide," Nat. Stand. Ref. Data Ser., Vol. 5, Nat. Bur. Stand. U.S., Washington, DC, 1966.
2. G. H. DIEKE AND J. W. MAUCHLY, *Phys. Rev.* **43,** 12–30 (1933).
3. L. GERÖ, *Z. Phys.* **101,** 311–322 (1936).
4. R. SCHMID AND L. GERÖ, *Z. Phys.* **105,** 36–44 (1937).
5. J. KAPLAN, *Phys. Rev.* **35,** 1298L (1930).
6. R. SCHMID AND L. GERÖ, *Z. Phys.* **99,** 281–284 (1936).
7. C. V. V. PRASAD, G. L. BHALE, AND S. PADDI REDDY, *J. Mol. Spectrosc.* **121,** 261–269 (1987).
8. T. RYTEL, *J. Mol. Spectrosc.* **151,** 271–274 (1992).
9. A. O'KEEFE AND D. A. G. DEACON, *Rev. Sci. Instrum.* **59,** 2544 (1988).
10. G. MEIJER, M. G. H. BOOGAARTS, R. T. JONGMA, D. H. PARKER, AND A. M. WODTKE, *Chem. Phys. Lett.*, in press.
11. W. H. PRESS, B. F. FLANNERY, S. A. TEUKOLSKY, AND W. T. VETTERLING, "Numerical Recipes in C; the Art of Scientific Computing," Cambridge Univ. Press, Cambridge, 1988.
12. J. V. FOLTZ, D. H. RANK, AND T. A. WIGGINS, *J. Mol. Spectrosc.* **21,** 203–216 (1966).
13. S. GERSTENKORN AND P. LUC, "Atlas du spectroscopie d'absorption de la molecule d'iode," CRNS, Paris, 1978; *Rev. Phys. Appl.* **14,** 791–794 (1979).
14. T. C. JAMES, *J. Chem. Phys.* **55-8,** 4118–4124 (1971).
15. R. W. FIELD, S. G. TILFORD, R. A. HOWARD, AND J. D. SIMMONS, *J. Mol. Spectrosc.* **44,** 347–382 (1972).
16. A. W. MANTZ, J.-P. MAILLARD, WON B. ROH, AND K. NARAHARI RAO, *J. Mol. Spectrosc.* **57,** 155–159 (1975).
17. T. J. MCGEE AND T. J. MCILRATH, *J. Quant. Spectrosc. Radiat. Transfer* **32-2,** 179–184 (1984).
18. I. KOVÁCS, "Rotational Structure in the Spectra of Diatomic Molecules," Adam Hilger Ltd., London, 1969.
19. V. HASSAN AND R. W. NICHOLLS, *J. Phys. B.* **4,** 681 (1971).